Biochemistry

Article

Cite This: Biochemistry 2019, 58, 1379−1387

pubs.acs.org/biochemistry

D1-S169A Substitution of Photosystem II Perturbs Water Oxidation

Ipsita Ghosh,[†] Gourab Banerjee,[†] Christopher J. Kim,[‡] Krystle Reiss,[†] Victor S. Batista,*[,†] Richard J. Debus,*[,‡] and Gary W. Brudvig*[,†]

[†]Department of Chemistry, Yale University, New Haven, Connecticut 06520-8107, United States

[‡]Department of Biochemistry, University of California, Riverside, California 92521, United States

Supporting Information

ABSTRACT: In photosystem II (PSII), photosynthetic water oxidation occurs at the tetramanganese−calcium cluster that cycles through light-induced intermediates (S_0−S_4) to produce oxygen from two substrate waters. The surrounding hydrogen-bonded amino acid residues and waters form channels that facilitate proton transfer and substrate water delivery, thereby ensuring efficient water oxidation. The residue D1-S169 lies in the "narrow" channel and forms hydrogen bonds with the Mn_4CaO_5 cluster via waters W1 and Wx. To probe the role of the narrow channel in substrate-water binding, we studied the D1-S169A mutation. PSII core complexes isolated from mutant cells exhibit inefficient S-state cycling and delayed oxygen evolution. The S_2-state multiline EPR spectrum of D1-S169A PSII core complexes differed significantly from that of wild-type, and FTIR difference spectra showed that the mutation strongly perturbs the extensive network of hydrogen bonds that extends at least from D1-Y161 (Y_Z) to D1-D61. These results imply a possible role of D1-S169 in proton egress or substrate water delivery.

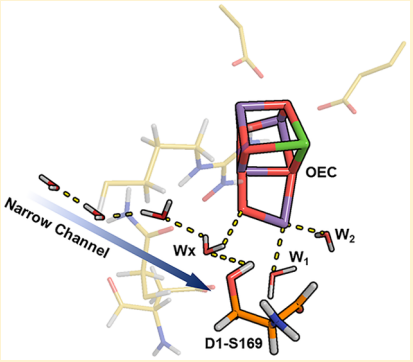

Water oxidation, a key step in oxygenic photosynthesis, is catalyzed by photosystem II (PSII), a protein complex embedded in the thylakoid membranes of cyanobacteria, algae, and higher plants.[1−6] As seen in the 1.9 Å crystal structure,[7] the PSII complex is composed of around 20 protein subunits including D1, D2, CP43, CP47, and cytochrome b-559. The catalytic center for water oxidation is the oxygen-evolving complex (OEC), consisting of a Mn_4CaO_5 cluster ligated by water, hydroxo/oxo species, and amino acid residues. In each turn of the catalytic cycle, the OEC oxidizes two H_2O molecules, forming O_2 via a light-driven cyclic process that cycles the metal cluster through intermediate oxidation states (the so-called storage (S) states of oxidizing equivalents, S_n states with n = 0−4). Protons released to the lumen by this process establish a pH gradient across the thylakoid membrane, while electrons extracted from water are used to reduce plastoquinone to plastoquinol.[1−6]

S-state cycling is initiated by light-induced charge separation between the reaction center chlorophyll molecules, P_{680}, and a nearby pheophytin molecule. $P_{680}^{\bullet+}$ is subsequently reduced by the redox-active tyrosine residue, Y_Z. The oxidized Y_Z drives single electron oxidations of the OEC, forming the redox intermediates of the Mn_4CaO_5 cluster.[1−6] The S-state intermediates have been characterized by different biophysical techniques, including extended X-ray absorption fine structure (EXAFS) spectroscopy, electron paramagnetic resonance (EPR) spectroscopy, and Fourier transform infrared (FTIR) spectroscopy.[1−6] EPR spectroscopy has been extensively used to characterize the S-state intermediates. The dark-stable S_1 state is integer spin and shows EPR signals in parallel mode, while the paramagnetic S_2 state can exist in the form of two spin isomers with effective spins of S_T = 1/2 and 5/2, respectively.[8] Under native conditions, in His-tagged *Synechocystis* PSII core complexes, an 18−22 multiline EPR signal is observed centered at g = 2. This multiline signal is characteristic of the S_T = 1/2 isomer where the Mn1, Mn2, Mn3, and Mn4 ions are in the III, IV, IV, and IV oxidation states, numbered as in Figure 1.[9] The light-driven oxidation of the S_3 state likely forms a transient S_4 intermediate that spontaneously evolves O_2 to regenerate the S_0 state. The water-oxidation mechanism is yet to be fully elucidated because of limited knowledge of the transient intermediates generated during the S_3 to S_0 transition.

Another unresolved aspect of the water-oxidation chemistry is the identification of the two substrate water molecules. Both are already bound in the S_2 state,[10] and one may relocate during the S_2 to S_3 transition. Though the structures of both the S_2 and S_3 states are well-characterized, there is an ongoing debate regarding the mechanism of S_3-state formation and the identity of the substrate water molecule that relocates. The hydrogen-bonding interactions with the neighboring waters and amino acid residues are crucial in maintaining the pK_a of the substrate waters.[3] Hence, a few point mutations have been generated to study a putative substrate-water delivery channel.[11] The identification of the substrate water molecules will help to resolve the two most debated mechanisms of

Received: November 13, 2018
Revised: January 11, 2019
Published: February 1, 2019

DOI: 10.1021/acs.biochem.8b01184
Biochemistry 2019, 58, 1379−1387

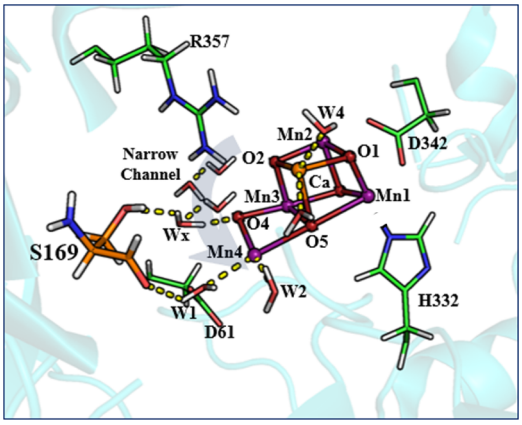

Figure 1. Structure of the OEC depicting the hydrogen-bonding network connecting D1-S169 (in orange), Wx, and O4 in cyanobacterial PSII based on the crystal structure (PDB 3WU2).[7] The Mn atoms are marked in purple, Ca in light orange, C atoms in green, N atoms in blue, and O atoms in red.

oxygen formation: water-nucleophilic attack and oxo-oxyl radical mechanisms.[12,13]

The OEC is surrounded by a hydrogen-bonded network of water molecules and amino acid residues that have been classified into channels referred to as the large, broad, and narrow channels.[2,14,15] These channels are thought to play crucial roles in proton transfer to the lumen and substrate water delivery to the Mn cluster. Mutational analyses have been performed to characterize the proton-transfer pathway(s). These studies include mutations of D2-K317, D1-D61, D1-E65, D1-R334, and D1-E333 that resulted in inefficient S-state cycling, delay of oxygen evolution, and/or alteration of the decay kinetics of the S states.[11,16−22] These residues lie in the broad channel that has been designated as a proton-exit channel that functions during at least the S_3 to S_0 transition.[14,15,23] Further, it has been observed that modulation of the chloride-binding site present in the broad channel can also influence the proton-transfer process.[24] Ishikita and co-workers have further proposed that the narrow channel involving O4 is involved in deprotonation during the S_0−S_1 transition.[25]

There are differing proposals regarding the substrate water delivery pathway.[3] Ammonia, a substrate water analogue, binds to Mn4, which is located near the terminus of the narrow channel.[26−28] Further, another substrate water analogue, methanol, binds in this channel near Mn4 and O4.[29−32] These results along with molecular dynamics simulations strongly suggest the narrow channel as the substrate water delivery channel. On the other hand, the water cavity in the large channel involving W3 was perturbed by the D1-V185N mutation.[11,33] On the basis of these and other studies and computational analyses, the large channel has been proposed as the substrate water delivery channel with W3 acting as one of the substrate waters.[11,33−37]

In this study, we investigate the substrate-water delivery pathway by perturbing the surrounding hydrogen-bonding network connecting the narrow channel around Mn4. The residue D1-S169 lies in the narrow channel and is hydrogen bonded to W1 (ligated to Mn4) through its backbone and Wx (ligated to O4) through its side chain (Figure 1). Hence, to study the role of these waters and the narrow channel in the substrate delivery process, we constructed the D1-S169A mutation. The characteristics of water oxidation exhibited by D1-S169A mutated PSII provide new insight into the identity of the substrate waters and the mechanism of substrate water binding to the OEC during the S_2 to S_3 transition.

MATERIALS AND METHODS

Construction of Mutants and Isolation of PSII Core Complexes. The D1-S169A mutation was introduced into the psbA-2 gene of *Synechocystis* sp. PCC 6803 and transformed into a host strain of *Synechocystis* that lacks all three psbA genes and contains a hexa-histidine tag (His-tag) fused to the C-terminus of CP47.[38] The cultures were maintained and propagated as described previously.[20] Oxygen-evolving PSII core complexes were purified under dim green light at 4 °C with a Ni-NTA superflow affinity resin (Qiagen, Valencia, CA) as described previously.[39] The purified PSII core complexes were finally suspended in buffer containing 1.2 M betaine, 10% (v/v) glycerol, 50 mM MES-NaOH (pH 6.0), 20 mM $CaCl_2$, 5 mM $MgCl_2$, 50 mM histidine, 1 mM EDTA, and 0.03% (w/v) *n*-dodecyl β-D-maltoside, frozen in liquid N_2, and stored at 77 K. To verify the integrity of the mutant cultures, sequencing of the relevant portion of the psbA-2 gene was performed after polymerase chain reaction amplification of genomic DNA.[18] No traces of the wild-type codon were detected in any of the mutant cultures.

Steady-State Oxygen-Evolution Assays. Oxygen evolution from purified PSII core complexes of His-tagged wild-type and D1-S169A mutated PSII was monitored with a Clark-type electrode as described previously.[18] The assay buffer contained 1 M sucrose, 50 mM MES-NaOH (pH 6.5), 50 mM $CaCl_2$, and 10 mM NaCl. Then, 250 μM PPBQ and 1 mM $K_3[Fe(CN)_6]$ were used as electron acceptors, and 5 μg of Chl was used for each assay.

Polarographic Oxygen-Evolution Measurements. Flash-induced O_2 yields of PSII core complexes of His-tagged wild-type and the D1-S169A mutant were measured using a bare platinum electrode.[40] The samples were suspended in buffer containing 1 M sucrose, 10 mM $CaCl_2$, 200 mM NaCl, and 50 mM MES-NaOH (pH 6.50) as described previously.[40] Then, 500 μM DCBQ and 1 mM K_3FeCN_6 were added as electron acceptors. The oscillations resulting from 20 flashes were fit to the VZAD model[41] to obtain the corresponding miss parameters, hits, and double hits. An interval spacing of 1 s was used to collect data for flash oxygen kinetics.

Electron Paramagnetic Resonance Studies. EPR samples were prepared in a buffer containing 50 mM MES-NaOH (pH 6.0), 1 M sucrose, 20 mM $CaCl_2$, 5 mM $MgCl_2$, and 1 mM EDTA and concentrated to 1 mg of Chl/mL using Amicon centrifugal cells having a 100 kDa cutoff. The measurements were performed using a Bruker ELEXSYS E500 spectrometer equipped with a SHQ resonator and an Oxford ESR-900 continuous flow cryostat at 7.5 K. The EPR parameters used for recording the spectra are as follows: microwave frequency, 9.38 GHz; modulation frequency, 100 kHz; modulation amplitude, 19.95 G; microwave power, 5 mW; sweep time, 84 s; conversion time, 41 ms; time constant, 82 ms. Each spectrum is the average of two scans. The dark scan of the EPR samples, concentrated to 1 mg of Chl/mL, corresponding to the S_1 state was recorded. The S_2 state was generated by illuminating the sample with a Xe lamp in a 200 K acetone/dry ice bath for 5 min, and the spectrum was recorded.

DOI: 10.1021/acs.biochem.8b01184
Biochemistry 2019, 58, 1379−1387

FTIR Measurements. Samples were prepared as described previously[18] except that they were maintained at a relative humidity of 95% with droplets of 40% (v/v) glycerol in water. Spectra were obtained as described previously[21] with a Bruker Vertex 70 spectrometer (Bruker Optics, Billerica, MA) containing a preamplified, midrange D317 photovoltaic MCT detector (Kolmar Technologies, Inc., Newburyport, MA). For each sample, the absorbance at 1657 cm^{-1} (amide I band) was 0.6−1.1. After preflashing and dark adaptation, samples were illuminated at 0 °C with six flashes at 13 s intervals. Two transmission spectra (each consisting of 100 scans) were recorded before the first flash, and one transmission spectrum was recorded after the first and subsequent flashes. The difference spectra of the successive S-state transitions (e.g., $S_{n+1}-S_n$ difference spectra, henceforth written $S_{n+1} - S_n$) were obtained by dividing the transmission spectrum obtained after the *n*th flash by the transmission spectrum obtained before the *n*th flash and then converting the ratio to units of absorption. The baseline stability/noise level was obtained by dividing the second preflash transmission spectrum by the first and converting the ratio to units of absorption. (These spectra are labeled dark−dark in each figure.) The sample was then dark-adapted for 30 min, and the cycle was repeated. For each sample, the illumination cycle was repeated up to 15 times. The spectra of 20−22 samples were averaged (see figure legends).

QM/MM Calculations. The QM/MM computational model of the oxygen-evolving complex (OEC) was constructed as described in previous work.[42,43] Residues in the model included those with C_α within 15 Å of the OEC. The two chloride anions and all water molecules whose oxygen atoms fall within this boundary were also included. Cut residues were capped with neutral backbone fragments (ACE/NME), whose position was dictated by the location the neighboring residues.

Residues included in the model are listed as follows, with capping residues only including the backbone atoms indicated by parentheses:

D1 (chain A): (57)-58−67-(68), (81)-82−91-(92), (107)-108−112-(113), (155)-156−192-(193), (289)-290−298-(299), (323)-324−344, C-terminus.

CP43 (chain C): (290)-291-(292), (305)-306-314-(315), (334)-335−337-(338), (341)-342-(343), (350)-351−358-(359), (398)-399−402-(403), (408)-409−413-(414).

D2 (chain D): (311)-312−321-(322), (347)-348−352, C-terminus.

The model was optimized as a two-layer QM/MM model using the ONIOM[44] method as implemented in the Gaussian 09[45] software suite. The QM layer included the OEC, surrounding residues (D1-D170, D1-E189, D1-H332, D1-E333, D1-D342, CP43-E354, the C-terminus of D1-A344, D1-H337, CP43-R357, and D1-D61), and 10 bound water molecules. Clipped side chains were modeled as described previously.[43] The QM layer was calculated at the B3LYP[46,47] level of theory, with the LanL2DZ[48] basis set and pseudopotentials used for Mn and Ca atoms, 6-31G[49] for C, N, and H, and 6-31G(d)[50] for O. The lower MM layer was calculated using the AMBER[51] force field. All atoms were allowed to relax, excluding the capping residues and the chloride and oxygen atoms of waters in the MM layer.

RESULTS

D1-S169A cells are photoautotrophic and evolve oxygen at 77 ± 7% the rate of wild-type cells under light-saturated conditions (Table S1). The PSII content of D1-S169A cells was estimated to be 111 ± 5% compared to wild-type cells on the basis of measurements of the maximum fluorescence yields ($F_{max} - F_0$) of wild-type and D1-S169A cells (Figure S1 and Supplementary Note S1). It was estimated that 10−14% of the PSII reaction centers in D1-S169A cells lack Mn_4CaO_5 clusters *in vivo* on the basis of measurements of the kinetics of charge recombination between $Q_A^{\bullet-}$ and the donor side of PSII following 5 s of illumination in the presence of DCMU (Figure S2 and Supplementary Note S1). The presence of PSII reaction centers lacking Mn_4CaO_5 clusters implies that the cluster is assembled less efficiently or is less stable in D1-S169A cells compared to wild-type cells. The active fraction of PSII reaction centers in D1-S169A cells has a lower light-saturated rate of oxygen evolution compared to wild-type cells, especially when normalized to the higher PSII content of D1-S169A cells. If O_2 comes from 85 to 90% of the mutant PSII core complexes in the cells (see above), the normalized O_2 activity relative to WT would be 76−81%, implying that the efficiency of the S-state cycle is somewhat impaired in the mutant. In D1-S169A cells, the kinetics of charge recombination between $Q_A^{\bullet-}$ and the donor side of PSII following a single flash given in the presence of DCMU were slightly slower than those of wild-type cells, implying a slight decrease in the S_2/S_1 midpoint potential in the mutant cells (Figure S2 and Table S1).

PSII core complexes isolated from the D1-S169A mutant cells exhibited a maximal light-saturated oxygen-evolution rate of 1330 ± 28 μmol of O_2/(mg of Chl·hr), approximately 47% that of wild-type PSII. The lower relative activity compared to intact cells may be caused by loss of Mn_4CaO_4 clusters during purification or by a further diminished efficiency of S-state cycling under the conditions of the measurements of the D1-S169A PSII core complexes. To characterize the turnover efficiency of D1-S169A PSII core complexes, we compared the flash O_2-yield patterns of wild-type and D1-S169A PSII core complexes in response to 20 saturating flashes given at 23 °C. These patterns show highly damped flash-induced oscillations for D1-S169A PSII core complexes. The miss probability (α) is 2.2 times higher than that of wild-type PSII core complexes (Figure 2, Table 1), showing a decreased S-state cycling efficiency. Further, we observed a delay in the oxygen-evolution kinetics for D1-S169A PSII core complexes (Figure 3). Taken together, these studies indicate that the D1-S169A mutation diminishes the efficiency of water oxidation.

FTIR Characterization. The midfrequency FTIR difference spectra produced by the first, second, third, and fourth flashes given to wild-type PSII core complexes correspond predominantly to the S_2-S_1, S_3-S_2, S_0-S_3, and S_1-S_0 FTIR difference spectra, respectively.[22,52,53] Spectra from wild-type and D1-S169A PSII core complexes are compared in Figure 4. The amplitudes of the D1-S169A spectra produced by the first and second flashes are considerably lower than those of the corresponding spectra of wild-type (upper two sets of traces) on a protein basis (the spectra were normalized to the amplitudes of their absolute absorbances at 1657 cm^{-1}) but are recognizable as corresponding predominantly to S_2-S_1 and S_3-S_2 spectra, respectively. The D1-S169A spectra produced by the third and fourth flashes (lower two red traces in Figure 4) exhibit a few recognizable features. The indistinct nature of the mutant spectra produced by the third and fourth flashes may reflect the much higher miss parameter measured polarographically in D1-S169A PSII core complexes.

DOI: 10.1021/acs.biochem.8b01184
Biochemistry 2019, 58, 1379−1387

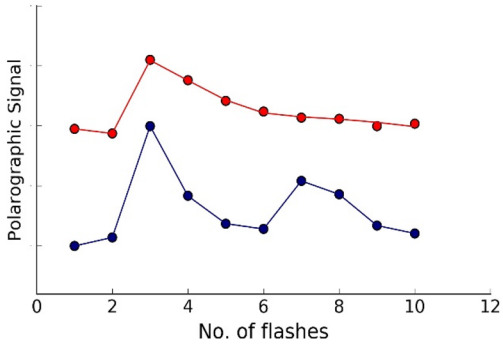

Figure 2. Comparison of the flash oxygen-yield patterns of PSII core complexes from His-tagged wild-type *Synechocystis* (blue) and D1-S169A (red). The data from wild-type and D1-S169A PSII are offset vertically for clarity. The oscillations resulting from 20 flashes at 23 °C were fit to the VZAD model to obtain the corresponding miss parameters, hits, and double hits.[41] Table 1 shows the Kok-model fitting parameters for wild-type and D1-S169A PSII core complexes. Average values from 3 independent experiments are reported. The standard errors are calculated. The S-state percentages have standard errors of ±5%.

Table 1. Kok-Model Fitting Parameters

parameter	wild-type	D1-S169A
misses, α (%)	14 ± 1	31 ± 2
double hits, β (%)	3 ± 1	4 ± 1
S_0 (%)	15	2
S_1 (%)	52	64
S_2 (%)	21	14
S_3 (%)	13	20

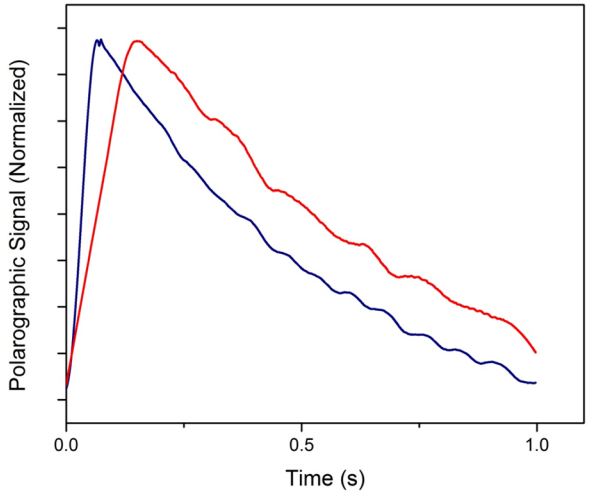

Figure 3. Comparison of the O_2-release kinetics of D1-S169A (red) and wild-type (blue) PSII core complexes. The peak values for oxygen evolution are normalized to facilitate comparison. The S169A core complexes exhibited a maximal oxygen-evolution rate of 1330 ± 28 μmol of O_2/(mg of Chl·hr), approximately 47% that of wild-type PSII.

The midfrequency S_2-S_1 spectrum of D1-S169A showed substantial changes compared to the wild-type throughout the midfrequency region. In the amide I region, a negative feature appeared at 1641 cm^{-1} and the 1680(−) cm^{-1} and 1622(+) cm^{-1} features were eliminated or nearly eliminated, respectively. These features can be assigned to amide I modes because they are sensitive to global ^{13}C labeling but not to

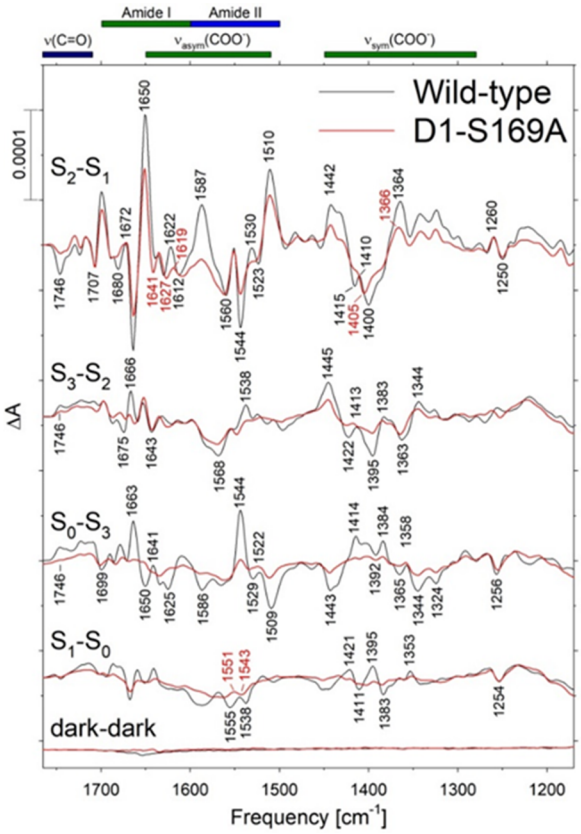

Figure 4. Comparison of the midfrequency FTIR difference spectra of wild-type (gray) and D1-S169A (red) PSII core complexes in response to four successive flash illuminations applied at 0 °C. The data (plotted from 1770 to 1170 cm^{-1}) represent the averages of 22 wild-type and 20 D1-S169A samples (33000 and 29600 scans, respectively). The spectra have been normalized to the average absolute amplitudes of the samples at the amide I peak at 1657 cm^{-1}. Dark−dark traces show the noise level and the stability of the baseline.

global ^{15}N labeling.[54,55] In the asymmetric carboxylate stretching [$\nu_{asym}(COO^-)$] and amide II region, the 1587(+) cm^{-1} feature was nearly eliminated, the 1544(−) cm^{-1} feature was diminished, and the 1530(+)/1523(−) cm^{-1} derivative feature was abolished. The 1587 cm^{-1} feature corresponds to a $\nu_{asym}(COO^-)$ mode because it is sensitive to global ^{13}C labeling[54,56−58] but not to global ^{15}N labeling.[16,54,56,58,59] The 1544(−) and 1530(+)/1523(−) cm^{-1} features correspond to amide II modes because they are sensitive to both global ^{13}C labeling[54,56−58] and global ^{15}N labeling.[16,54,56,58,59] In the symmetric carboxylate stretching [$\nu_{sym}(COO^-)$] region, the 1415(−)/1410(+) cm^{-1} derivative feature was eliminated and the 1400(−) cm^{-1} feature was upshifted by 5 cm^{-1}. Finally, in the carbonyl stretching [$\nu(C{=}O)$] region, the 1746(−) cm^{-1} feature was diminished. The midfrequency S_3-S_2 spectrum of D1-S169A also showed changes throughout the midfrequency region. The 1675(−)/1666(+) cm^{-1} derivative feature in the amide I region was eliminated, the 1538(+) cm^{-1} feature in the $\nu_{asym}(COO^-)$/amide II region was eliminated, the 1422(−)/1413(+) cm^{-1} derivative feature in the $\nu_{sym}(COO^-)$ region was eliminated and the 1363(−) cm^{-1} and 1344(+) cm^{-1} features were upshifted slightly.

The O−H stretching vibrations of strongly H-bonded OH groups can be observed as very broad positive features between

DOI: 10.1021/acs.biochem.8b01184
Biochemistry 2019, 58, 1379−1387

3200 and 2500 cm^{-1}.[21,22,60,61] These regions of the S_n-S_{n-1} difference spectra of D1-S169A PSII core complexes are compared with wild-type PSII core complexes in Figure 5A. In

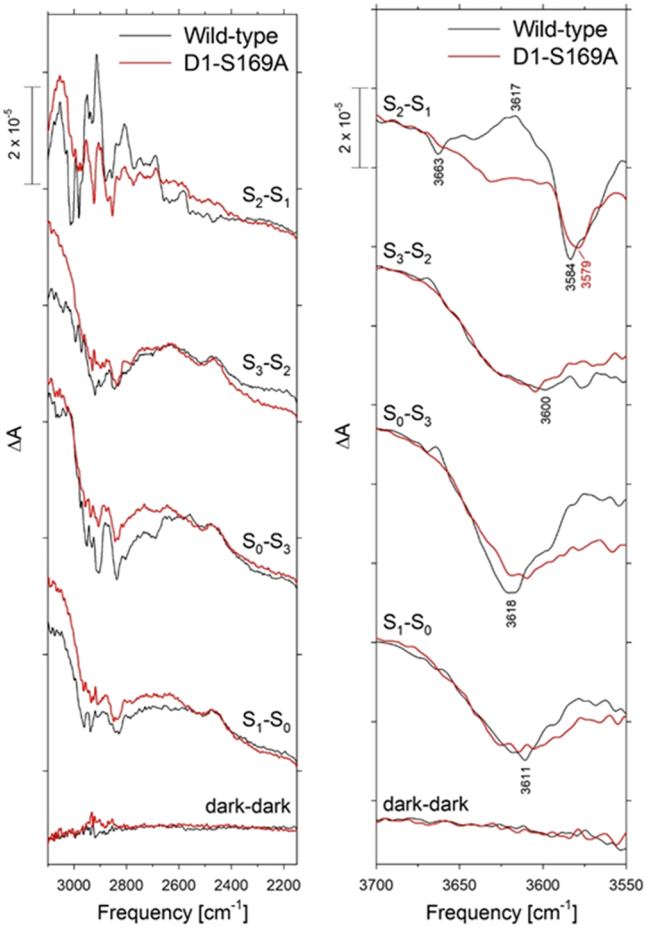

Figure 5. (A) Comparison of the strongly hydrogen-bonded O−H stretching region of wild-type (gray) and D1-S169A (red) PSII core complexes in response to four successive flash illuminations applied at 0 °C. The data were collected simultaneously with those in Figure 4. (B) Comparison of the weakly hydrogen-bonded O−H stretching region of wild-type and D1-S169A PSII core complexes in response to four successive flash illuminations applied at 0 °C. The data were collected simultaneously with those in Figure 4.

the S_2-S_1 spectrum, the broad feature is overlain with positive features that have been attributed to the N−H stretching vibration of the protonated D1-H337 side chain.[62] The broad feature of the S_2-S_1 spectrum was substantially altered by the D1-S169A mutation: much of the amplitude in the 3000−2700 cm^{-1} region appeared downshifted to between 2700 and 2400 cm^{-1} (upper pair of traces in Figure 5A).

In contrast, the broad feature of the S_3-S_2 spectrum was largely unaltered by the mutation. The apparent mutation-induced alterations to the broad features produced by the third and fourth flashes may arise from significant contributions of the mutant S_2-S_1 and S_3-S_2 spectra to these spectra because of the high miss parameter in D1-S169A PSII core complexes.

The O−H stretching vibrations of weakly hydrogen-bonded OH groups of water molecules can be observed between 3700 and 3500 cm^{-1}.[22,52,53,61] In the S_2-S_1 spectrum, the D1-S169A mutation eliminated the small 3663(−) cm^{-1} and large 3617(+) cm^{-1} features and shifted the 3584(−) cm^{-1} feature to 3579 cm^{-1} (Figure 5B, upper traces). The mutation had no apparent effect on the broad negative feature in the S_3-S_2 spectrum (Figure 5B, second set of traces). Any apparent mutation-induced alteration to the broad features produced by the third and fourth flashes may arise from significant contributions of the mutant S_2-S_1 and S_3-S_2 spectra to these spectra because of the mutated sample's high miss parameter.

The fraction of PSII containing functional Mn_4CaO_5 clusters in PSII core complexes was estimated from the $S_2 - S_1$ FTIR difference spectra. The lower amplitudes of the peaks at 1664(−), 1650(+), 1510(+), 1442(+), and 1400(−) in the D1-S169A spectrum suggest that approximately 60% of the mutant PSII core complexes contain Mn_4CaO_5 clusters capable of reaching the S_2 state. On the basis of the amplitude of the O_2 flash yield on the third flash (Figure 2), we estimate that 67% of mutant PSII core complexes contain Mn_4CaO_5 clusters capable of making O_2. The steady-state O_2 forming rate of the mutant PSII cores was 47% compared to WT. Consequently, the normalized O_2 activity of D1-S169A PSII core complexes relative to WT would be 70−78%, similar to the 76−81% estimate in D1-S169A cells (see above), suggesting that the lower efficiency of O_2 evolution is similar in both cells and PSII core complexes.

EPR Characterization. To analyze the structure of the OEC, cw-EPR spectra of the S_2 states of both D1-S169A and wild-type PSII core complexes were collected (Figure S3, Figure 6). The S_2-state spectrum of wild-type PSII exhibits an

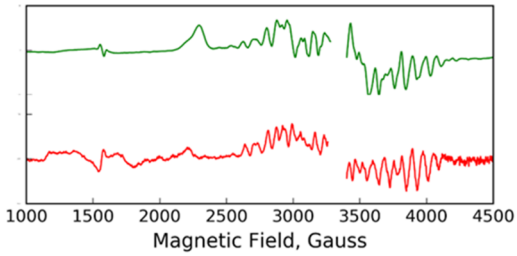

Figure 6. Comparison of the S_2-S_1 state difference EPR spectra of wild-type (green) and D1-S169A PSII core complexes (red). The unsubtracted spectra are reported in Figure S3.

18−22 multiline EPR signal centered at $g = 2$, corresponding to the $S_T = 1/2$ spin state isomer. This multiline signal has an average hyperfine line spacing of ∼87.5 G, consistent with previously reported values in the literature.[63]

The cw-EPR spectrum of the S_2 state of D1-S169A PSII also exhibits a multiline signal centered at $g = 2$. However, the average hyperfine line spacing of the multiline signal is reduced to ∼72 G, which suggests alterations in the structure of the OEC.

QM/MM Calculations on the S_1 State of D1-S169A. The D1-S169 residue is part of the narrow channel, and therefore, substitution of this residue can affect the substrate water delivery to OEC. The QM/MM minimized structure of the D1-S169A mutant in the S_1 state revealed that the elimination of the hydrogen bond between D1-S169 and Wx caused Wx to shift by 0.5 Å and W195 by 0.3 Å toward the narrow channel. We also see slight movement in CP43-R357 and D1-D61 (0.18 and 0.12 Å, respectively) as the two residues equilibrate to the new location of Wx (Figure 7). A disruption in the substrate-water delivery is consistent with the

DOI: 10.1021/acs.biochem.8b01184
Biochemistry 2019, 58, 1379−1387

observed impairment of S-state cycling in D1-S169A PSII as well as delayed oxygen evolution.

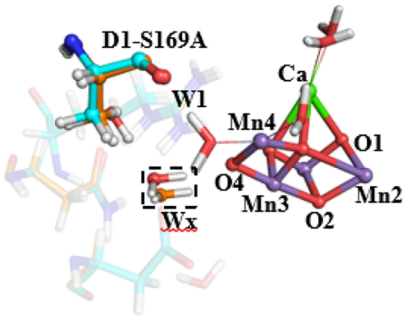

Figure 7. Superposition of the QM/MM optimized structures of wild-type (blue) and D1-S169A PSII (orange) in the S_1 state. The dashed box indicates the shift in Wx (red, in wild-type PSII).

DISCUSSION

The narrow channel has been proposed previously to be the substrate-water delivery channel[29] and to play an important role in proton egress.[25] Hence, we substituted a narrow channel residue D1-S169 with A169 to study the effect of perturbation of the hydrogen-bonding network involving Wx, W1, O4, and Mn4. PSII core complexes isolated from D1-S169A cells exhibit reduced oxygen evolution and impaired S-state cycling. Similar characteristics have often been displayed by PSII core complexes of secondary shell mutants including D2-K317A,[16] D1-D61A,[21] CP43-R357K,[64] and D1-N87D.[24] These perturbations were caused by alterations to the hydrogen-bonding network around the OEC, presumably resulting in a hindered proton transfer.[19−22,29,33]

The substantial D1-S169A mutation-induced changes to the midfrequency S_2-S_1 FTIR difference spectrum show that the D1-S169A mutation alters the response of carboxylate groups and the protein backbone to the positive charge that develops on the Mn_4CaO_5 cluster during the S_1 to S_2 transition. Similar alterations are produced by mutations of numerous residues that are located in the networks of hydrogen bonds that surround the Mn_4CaO_5 cluster. Examples include D1-D61A,[21] D1-E65A,[19] D1-N87A,[24] D1-Q165E,[20] D1-N181A,[18] D1-V185N,[33] D1-N298A,[65] D1-R334A,[20] D2-E312A,[19] and D2-K317A.[16] The diminished amplitudes of the carbonyl, carboxylate, and amide II features at 1746(−) cm^{-1}, 1587(+) cm^{-1}, and 1544(−) cm^{-1}, respectively, in the S_2-S_1 FTIR difference spectrum are also produced by the D1-D61A, D1-E65A, D1-V185N, D1-N298A, D2-E312Q, and D1-R334A mutations.[19−21,33,65] These spectral changes may reflect similar perturbations of the polypeptide backbone that are caused by disruption of the same network of hydrogen bonds. The 1530(+)/1522(−) cm^{-1} feature in the S_2-S_1 difference spectrum that is eliminated by the D1-S169A mutation is also eliminated by the D1-D61A,[21] D1-E65A,[19] D1-N181A,[18] D1-V185N,[33] D1-N298A,[65] D1-R334A,[20] D2-E312A,[19] and D2-K317A mutations.[16] Elimination of the same feature by mutations constructed at these eight residues implies that each mutation partly disrupts a common network of hydrogen bonds that includes the nearby Cl^- ion. The spectral changes produced by the D1-S169A mutation in the midfrequency region are, therefore, consistent with the participation of D1-S169 in a network of hydrogen bonds that forms a water entry channel, leading to the Mn_4CaO_5 cluster and/or a proton-exit pathway.

In the strongly hydrogen-bonded O−H stretching region, the broad positive feature observed in the S_2-S_1 spectrum between 3100 and 2400 cm^{-1} has been assigned to the coupled O−H stretching vibrations of strongly hydrogen-bonded water molecules in an extended network of hydrogen bonds that links D1-D61 with the Ca^{2+} ion and Y_Z.[61] This feature is dominated by the O−H stretching vibrations of W1 and W2[61] and is eliminated by the D1-D61A mutation.[21] That D1-S169A also alters this feature implies that D1-S169 participates in the same hydrogen-bonding network. Such participation would be consistent with the 1.9 Å X-ray crystallographic structures; in these structures, D1-S169 forms a hydrogen bond with a water molecule that also forms hydrogen bonds with D1-D61 and the O4 oxo bridge of the Mn_4CaO_5 cluster.[7,66,67]

In the weakly hydrogen-bonded O−H stretching region, the features observed in the S_2-S_1 spectrum between 3700 and 3500 cm^{-1} have been assigned to the coupled O−H stretching vibrations of weakly hydrogen-bonded water molecules in the same extended network of hydrogen bonds mentioned above.[61] The small 3663(−) cm^{-1} feature that is eliminated by the D1-S169A mutation is also eliminated by the D1-D61A,[21] D1-N298A,[65] and D1-E333Q[68] mutations. The feature is also diminished by the D1-N181A mutation.[18] The larger 3617(+) cm^{-1} feature that is eliminated by the D1-S169A mutation is also eliminated by the D1-D61A,[21] D1-N87A,[24] and D1-V185N[33] mutations and is diminished by the D1-N181A[18] mutation and also by the substitution of Sr^{2+} for Ca^{2+}.[34] Consequently, the spectral features altered by the D1-S169A mutation in the strongly and weakly hydrogen-bonded O−H stretching regions are consistent with D1-S169 participating in an extensive network of hydrogen bonds involved in water entry and/or proton egress.

To understand the changes in the structure of the OEC, EPR studies were carried out. EPR studies demonstrated that the S_2 state multiline EPR signal was altered in D1-S169A PSII. The lower intensity of the multiline EPR signal in D1-S169A PSII is a consequence of both the lower fraction of PSII centers having assembled/functional metal clusters in the mutant and the altered hyperfine splittings in the mutant. Similar alterations to the S_2 state multiline EPR signal have been observed in PSII depleted of Ca^{2+},[69] in PSII having Ca substituted by Sr,[70,71] in ammonia-treated PSII,[26−28,72] in PSII from the D1-H332E mutant,[73] and in PSII from the D1-D61A mutant,[26] another secondary shell mutation. Pulsed EPR studies have shown that these spectral changes are caused by slight alterations to the environment of the S_2 state's single Mn(III) ion, caused in turn by treatment/mutation-induced alterations to the magnetic couplings between the individual Mn ions.[28,69,71,73] The alterations to the multiline signal caused by the D1-D61A mutation can be attributed to perturbations of hydrogen bonds involving Mn4. The alterations caused by the D1-S169A mutation likely have the same origin. Such an interpretation is in good agreement with the QM/MM analyses, which show that the waters in the narrow channel ligated to the cluster (Wx) are affected as a result of the D1-S169A site-directed mutation. It has been shown in a recent publication that the waters in the narrow channel in wild-type PSII remain unperturbed, except W20 (here the water hydrogen bonded to Wx), which disappears in the S_2 and S_3 states.[74] However, in the D1-S169A mutant, we do observe movement of waters in the narrow channel in the S_1 state,

DOI: 10.1021/acs.biochem.8b01184
Biochemistry 2019, 58, 1379−1387

which is possibly a consequence of the mutation. Hence, on the basis of these results, it will be interesting to further probe the disappearance of W20 and understand its role in the substrate water delivery mechanism. In our previous studies, we have observed intricate connections between the channels,[24] and thereby, we do not negate the possibility that the mutations in the narrow channel result in hindrance of substrate water delivery through the large channel. The impaired S-state cycling and the delayed oxygen kinetics can be the consequence of a hindered substrate water channel, changes in the substrate water binding mechanism, or partial disruption of proton egress. Further studies involving pulsed EPR techniques will be required to provide deeper insight into the nature of the perturbation of the Mn_4CaO_5 cluster by the D1-S169A mutation.

■ ASSOCIATED CONTENT

Supporting Information

The Supporting Information is available free of charge on the ACS Publications website at DOI: 10.1021/acs.biochem.8b01184.

Characteristics of wild-type and mutant cells; measurement of chlorophyll fluorescence and EPR spectra of the S_2 state and dark spectra (PDF)

■ AUTHOR INFORMATION

Corresponding Authors

*E-mail: victor.batista@yale.edu. Tel: (203) 432-6672. Fax: (203) 432-6144.
*E-mail: richard.debus@ucr.edu. Tel: (951) 827-3483. Fax: (951) 827-4294.
*E-mail: gary.brudvig@yale.edu. Tel: (203) 432-5202. Fax: (203) 432-6144.

ORCID

Victor S. Batista: 0000-0002-3262-1237
Richard J. Debus: 0000-0003-1321-8730
Gary W. Brudvig: 0000-0002-7040-1892

Author Contributions

The manuscript was written through contributions of all authors. All authors have given approval to the final version of the manuscript. I. Ghosh and G. Banerjee contributed equally.

Funding

This work was supported by grants from the Department of Energy, Office of Basic Energy Sciences, Division of Chemical Sciences. Oxygen-release and EPR studies were supported by grant no. DE-FG02-05ER15646 (to G.W.B.). Mutant construction and FTIR studies were supported by grant no. DE-SC0005291 (to R.J.D.). Computational studies were supported by grant no. DE-SC0001423 (to V.S.B.) and supercomputer time from NERSC.

Notes

The authors declare no competing financial interest.

■ REFERENCES

(1) Vinyard, D. J., Ananyev, G. M., and Dismukes, C. G. (2013) Photosystem II: the reaction center of oxygenic photosynthesis. *Annu. Rev. Biochem. 82*, 577−606.
(2) Vogt, L., Vinyard, D. J., Khan, S., and Brudvig, G. W. (2015) Oxygen-evolving complex of photosystem II: an analysis of second-shell residues and hydrogen-bonding networks. *Curr. Opin. Chem. Biol. 25*, 152−158.
(3) Vinyard, D. J., and Brudvig, G. W. (2017) Progress toward a molecular mechanism of water oxidation in photosystem II. *Annu. Rev. Phys. Chem. 68*, 101−116.
(4) Cox, N., and Messinger, J. (2013) Reflections on substrate water and dioxygen formation. *Biochim. Biophys. Acta, Bioenerg. 1827*, 1020−1030.
(5) Pérez-Navarro, M., Neese, F., Lubitz, W., Pantazis, D. A., and Cox, N. (2016) Recent developments in biological water oxidation. *Curr. Opin. Chem. Biol. 31*, 113−119.
(6) Pantazis, D. A. (2018) Missing pieces in the puzzle of biological water oxidation. *ACS Catal. 8*, 9477−9507.
(7) Umena, Y., Kawakami, K., Shen, J.-R., and Kamiya, N. (2011) Crystal structure of oxygen-evolving photosystem II at a resolution of 1.9 Å. *Nature 473*, 55−60.
(8) Pantazis, D. A., Ames, W., Cox, N., Lubitz, W., and Neese, F. (2012) Two interconvertible structures that explain the spectroscopic properties of the oxygen-evolving complex of photosystem II in the S_2 state. *Angew. Chem., Int. Ed. 51*, 9935−9940.
(9) Pokhrel, R., and Brudvig, G. W. (2014) Oxygen-evolving complex of photosystem II: correlating structure with spectroscopy. *Phys. Chem. Chem. Phys. 16*, 11812−11821.
(10) Nilsson, H., Krupnik, T., Kargul, J., and Messinger, J. (2014) Substrate water exchange in photosystem II core complexes of the extremophilic red alga *Cyanidioschyzon merolae*. *Biochim. Biophys. Acta, Bioenerg. 1837*, 1257−1262.
(11) Dilbeck, P. L., Bao, H., Neveu, C. L., and Burnap, R. L. (2013) Perturbing the water cavity surrounding the manganese cluster by mutating the residue D1-valine 185 has a strong effect on the water oxidation mechanism of photosystem II. *Biochemistry 52*, 6824−6833.
(12) Brudvig, G. W. (2008) Water oxidation chemistry of photosystem II. *Philos. Trans. R. Soc., B 363*, 1211−1219.
(13) Siegbahn, P. E. M. (2009) Structures and energetics for O_2 formation in photosystem II. *Acc. Chem. Res. 42*, 1871−1880.
(14) Bondar, A.-N., and Dau, H. (2012) Extended protein/water H-bond networks in photosynthetic water oxidation. *Biochim. Biophys. Acta, Bioenerg. 1817*, 1177−1190.
(15) Linke, K., and Ho, F. M. (2014) Water in photosystem II: structural, functional and mechanistic considerations. *Biochim. Biophys. Acta, Bioenerg. 1837*, 14−32.
(16) Pokhrel, R., Service, R. J., Debus, R. J., and Brudvig, G. W. (2013) Mutation of lysine 317 in the D2 subunit of photosystem II alters chloride binding and proton transport. *Biochemistry 52*, 4758−4773.
(17) Hundelt, M., Hays, A.-M., Debus, R. J., and Junge, W. (1998) Oxygenic photosystem II: The mutation D1-D61N in *Synechocystis* sp. PCC 6803 retards S-State transitions without affecting electron transfer from Y_Z to $P680^+$. *Biochemistry 37*, 14450−14456.
(18) Pokhrel, R., Debus, R. J., and Brudvig, G. W. (2015) Probing the effect of mutations of asparagine 181 in the D1 subunit of photosystem II. *Biochemistry 54*, 1663−1672.
(19) Service, R. J., Hillier, W., and Debus, R. J. (2010) Evidence from FTIR difference spectroscopy for an extensive network of hydrogen bonds near the oxygen-evolving Mn_4Ca cluster of photosystem II involving D1-Glu65, D2-Glu312, and D1-Glu329. *Biochemistry 49*, 6655−6669.
(20) Service, R. J., Hillier, W., and Debus, R. J. (2014) Network of hydrogen bonds near the oxygen-evolving Mn_4CaO_5 cluster of photosystem II probed with FTIR difference spectroscopy. *Biochemistry 53*, 1001−1017.
(21) Debus, R. J. (2014) Evidence from FTIR difference spectroscopy that D1-Asp61 influences the water reactions of the oxygen-evolving Mn_4CaO_5 cluster of photosystem II. *Biochemistry 53*, 2941−2955.
(22) Debus, R. J. (2015) FTIR studies of metal ligands, networks of hydrogen bonds, and water molecules near the active site Mn_4CaO_5 cluster in photosystem II. *Biochim. Biophys. Acta, Bioenerg. 1847*, 19−34.
(23) Vassiliev, S., Zaraiskaya, T., and Bruce, D. (2012) Exploring the energetics of water permeation in photosystem II by multiple steered

DOI: 10.1021/acs.biochem.8b01184
Biochemistry 2019, 58, 1379−1387

molecular dynamics simulations. *Biochim. Biophys. Acta, Bioenerg. 1817*, 1671−1678.
(24) Banerjee, G., Ghosh, I., Kim, C. J., Debus, R. J., and Brudvig, G. W. (2018) Substitution of the D1-Asn87 site in photosystem II of cyanobacteria mimics the chloride-binding characteristics of spinach photosystem II. *J. Biol. Chem. 293*, 2487−2497.
(25) Takaoka, T., Sakashita, N., Saito, K., and Ishikita, H. (2016) pK_a of a proton-conducting water chain in photosystem II. *J. Phys. Chem. Lett. 7*, 1925−1932.
(26) Oyala, P. H., Stich, T. A., Debus, R. J., and Britt, R. D. (2015) Ammonia binds to the dangler manganese of the photosystem II oxygen-evolving complex. *J. Am. Chem. Soc. 137*, 8829−8837.
(27) Perez Navarro, M. P., Ames, W. M., Nilsson, H., Lohmiller, T., Pantazis, D. A., Rapatskiy, L., Nowaczyk, M. M., Neese, F., Boussac, A., Messinger, J., et al. (2013) Ammonia binding to the oxygen-evolving complex of photosystem II identifies the solvent-exchangeable oxygen bridge (μ-oxo) of the manganese tetramer. *Proc. Natl. Acad. Sci. U. S. A. 110*, 15561−15566.
(28) Marchiori, D. A., Oyala, P. H., Debus, R. J., Stich, T. A., and Britt, R. D. (2018) Structural effects of ammonia binding to the Mn_4CaO_5 cluster of photosystem II. *J. Phys. Chem. B 122*, 1588−1599.
(29) Retegan, M., and Pantazis, D. A. (2016) Interaction of methanol with the oxygen-evolving complex: atomistic models, channel identification, species dependence, and mechanistic implications. *Chem. Sci. 7*, 6463−6476.
(30) Oyala, P. H., Stich, T. A., Stull, J. A., Yu, F., Pecoraro, V. L., and Britt, R. D. (2014) Pulse electron paramagnetic resonance studies of the interaction of methanol with the S_2 state of the Mn_4O_5Ca cluster of photosystem II. *Biochemistry 53*, 7914−7928.
(31) Nagashima, H., and Mino, H. (2017) Location of methanol on the S_2 state Mn cluster in photosystem II studied by proton matrix electron nuclear double resonance. *J. Phys. Chem. Lett. 8*, 621−625.
(32) Yata, H., and Noguchi, T. (2018) Mechanism of methanol inhibition of photosynthetic water oxidation as studied by Fourier transform infrared difference and time-resolved infrared spectroscopies. *Biochemistry 57*, 4803−4815.
(33) Kim, C. J., Bao, H., Burnap, R. L., and Debus, R. J. (2018) Impact of D1-V185 on the water molecules that facilitate O_2 formation by the catalytic Mn_4CaO_5 cluster in photosystem II. *Biochemistry 57*, 4299−4311.
(34) Kim, C. J., and Debus, R. J. (2017) Evidence from FTIR difference spectroscopy that a substrate H_2O molecule for O_2 formation in photosystem II is provided by the Ca ion of the catalytic Mn_4CaO_5 cluster. *Biochemistry 56*, 2558−2570.
(35) Shoji, M., Isobe, H., and Yamaguchi, K. (2015) QM/MM study of the S_2 to S_3 transition reaction in the oxygen-evolving complex of photosystem II. *Chem. Phys. Lett. 636*, 172−179.
(36) Ugur, I., Rutherford, A. W., and Kaila, V. R. (2016) Redox-coupled substrate water reorganization in the active site of photosystem II—the role of calcium in substrate water delivery. *Biochim. Biophys. Acta, Bioenerg. 1857*, 740−748.
(37) Isobe, H., Shoji, M., Shen, J.-R., and Yamaguchi, K. (2015) Strong coupling between the hydrogen bonding environment and redox chemistry during the S_2 to S_3 transition in the oxygen-evolving complex of photosystem II. *J. Phys. Chem. B 119*, 13922−13933.
(38) Debus, R. J., Campbell, K. A., Gregor, W., Li, Z.-L., Burnap, R. L., and Britt, R. D. (2001) Does histidine 332 of the D1 polypeptide ligate the manganese cluster in photosystem II? An electron spin echo envelope modulation study. *Biochemistry 40*, 3690−3699.
(39) Strickler, M. A., Walker, L. M., Hillier, W., and Debus, R. J. (2005) Evidence from biosynthetically incorporated strontium and FTIR difference spectroscopy that the C-terminus of the D1 polypeptide of photosystem II does not ligate calcium. *Biochemistry 44*, 8571−8577.
(40) Vinyard, D. J., and Brudvig, G. W. (2015) Insights into substrate binding to the oxygen-evolving complex of photosystem II from ammonia inhibition studies. *Biochemistry 54*, 622−628.
(41) Vinyard, D. J., Zachary, C. E., Ananyev, G., and Dismukes, G. C. (2013) Thermodynamically accurate modeling of the catalytic cycle of photosynthetic oxygen evolution: A mathematical solution to asymmetric Markov chains. *Biochim. Biophys. Acta, Bioenerg. 1827*, 861−868.
(42) Pal, R., Negre, C. F. A., Vogt, L., Pokhrel, R., Ertem, M. Z., Brudvig, G. W., and Batista, V. S. (2013) S_0-state model of the oxygen-evolving complex of photosystem II. *Biochemistry 52*, 7703−7706.
(43) Askerka, M., Wang, J., Brudvig, G. W., and Batista, V. S. (2014) Structural changes in the oxygen-evolving complex of photosystem II induced by the S_1 to S_2 transition: A combined XRD and QM/MM study. *Biochemistry 53*, 6860−6862.
(44) Vreven, T., and Morokuma, K. (2000) The ONIOM (our own N-layered integrated molecular orbital + molecular mechanics) method for the first singlet excited (S_1) state photoisomerization path of a retinal protonated Schiff base. *J. Chem. Phys. 113*, 2969−2975.
(45) Frisch, M. J., Trucks, G. W., Schlegel, H. B., Scuseria, G. E., Robb, M. A., Cheeseman, J. R., Scalmani, G., Barone, V., Petersson, G. A., Nakatsuji, H., Li, X., Caricato, M., Marenich, A. V., Bloino, J., Janesko, B. G., Gomperts, R., Mennucci, B., Hratchian, H. P., Ortiz, J. V., Izmaylov, A. F., Sonnenberg, J. L., Williams-Young, F., Ding, F., Lipparini, F., Egidi, F., Goings, J., Peng, B., Petrone, A., Henderson, T., Ranasinghe, D., Zakrzewski, V. G., Gao, J., Rega, N., Zheng, G., Liang, W., Hada, M., Ehara, M., Toyota, K., Fukuda, R., Hasegawa, J., Ishida, M., Nakajima, T., Honda, Y., Kitao, O., Nakai, H., Vreven, T., Throssell, K., Montgomery, J. A., Jr., Peralta, J. E., Ogliaro, F., Bearpark, M. J., Heyd, J. J., Brothers, E. N., Kudin, K. N., Staroverov, V. N., Keith, T. A., Kobayashi, R., Normand, J., Raghavachari, K., Rendell, A. P., Burant, J. C., Iyengar, S. S., Tomasi, J., Cossi, M., Millam, J. M., Klene, M., Adamo, C., Cammi, R., Ochterski, J. W., Martin, R. L., Morokuma, K., Farkas, O., Foresman, J. B., and Fox, D. J. (2016) *Gaussian 16*, Revision B.01, Gaussian, Inc., Wallingford, CT.
(46) Becke, A. D. (1988) Density-functional exchange-energy approximation with correct asymptotic behavior. *Phys. Rev. A: At., Mol., Opt. Phys. 38*, 3098−3100.
(47) Becke, A. D. (1993) Density-functional thermochemistry. III. The role of exact exchange. *J. Chem. Phys. 98*, 5648−5652.
(48) Hay, P. J., and Wadt, W. R. (1985) Ab initio effective core potentials for molecular calculations. Potentials for K to Au including the outermost core orbitals. *J. Chem. Phys. 82*, 299−310.
(49) Ditchfield, R., Hehre, W. J., and Pople, J. A. (1971) Self-consistent molecular-orbital methods 0.9. Extended Gaussian-type basis for molecular-orbital studies of organic molecules. *J. Chem. Phys. 54*, 724−728.
(50) Hariharan, P. C., and Pople, J. A. (1973) The influence of polarization functions on molecular orbital hydrogenation energies. *Theor Chim Acta. 28*, 213−222.
(51) Case, D. A., Darden, T. A., Cheatham, III, T. E., Simmerling, C. L., Wang, J., Duke, R. E., Luo, R., Walker, R. C., Zhang, W., Merz, K. M., Roberts, B., Hayik, S., Roitberg, A., Seabra, G., Swails, J., Götz, A. W., Kolossváry, I., Wong, K. F., Paesani, F., Vanicek, J., Wolf, R. M., Liu, J., Wu, X., Brozell, S. R., Steinbrecher, T., Gohlke, H., Cai, Q., Ye, X., Wang, J., Hsieh, M.-J., Cui, G., Roe, D. R., Mathews, D. H., Seetin, M. G., Salomon-Ferrer, R., Sagui, C., Babin, V., Luchko, T., Gusarov, S., Kovalenko, A., and Kollman, P. A. (2012) *AMBER 12*, University of California, San Francisco.
(52) Noguchi, T. (2008) Fourier transform infrared analysis of the photosynthetic oxygen-evolving center. *Coord. Chem. Rev. 252*, 336−346.
(53) Noguchi, T. (2013) Monitoring the reactions of photosynthetic water oxidation using infrared spectroscopy. *Biomed. Spectrosc. Imaging 2*, 115−128.
(54) Kimura, Y., Mizusawa, N., Ishii, A., Yamanari, T., and Ono, T-a. (2003) Changes of low-frequency vibrational modes induced by universal ^{15}N-and ^{13}C-isotope labeling in S_2/S_1 FTIR difference spectrum of oxygen-evolving complex. *Biochemistry 42*, 13170−13177.

DOI: 10.1021/acs.biochem.8b01184
Biochemistry 2019, 58, 1379−1387

(55) Mizusawa, N., Yamanari, T., Kimura, Y., Ishii, A., Nakazawa, S., and Ono, T.-a. (2004) Changes in the functional and structural properties of the Mn cluster induced by replacing the side group of the C-terminus of the D1 protein of photosystem II. *Biochemistry 43*, 14644−14652.
(56) Yamanari, T., Kimura, Y., Mizusawa, N., Ishii, A., and Ono, T.-a. (2004) Mid-to low-frequency Fourier transform infrared spectra of S-state cycle for photosynthetic water oxidation in *Synechocystis* sp. PCC 6803. *Biochemistry 43*, 7479−7490.
(57) Noguchi, T., Sugiura, M., and Inoue, Y. (1999) *FTIR studies on the amino-acid ligands of the photosynthetic oxygen-evolving Mn-cluster. Fourier Transform Spectroscopy: Twelfth International Conference*, pp 459−460, Waseda University Press, Tokyo, Japan.
(58) Noguchi, T., and Sugiura, M. (2003) Analysis of flash-induced FTIR difference spectra of the S-state cycle in the photosynthetic water-oxidizing complex by uniform ^{15}N and ^{13}C isotope labeling. *Biochemistry 42*, 6035−6042.
(59) Service, R. J., Yano, J., McConnell, I., Hwang, H. J., Niks, D., Hille, R., Wydrzynski, T., Burnap, R. L., Hillier, W., and Debus, R. J. (2011) Participation of glutamate-354 of the CP43 polypeptide in the ligation of Mn and the binding of substrate water in photosystem II. *Biochemistry 50*, 63−81.
(60) Noguchi, T., and Sugiura, M. (2002) FTIR detection of water reactions during the flash-induced S-state cycle of the photosynthetic water-oxidizing complex. *Biochemistry 41*, 15706−15712.
(61) Nakamura, S., Ota, K., Shibuya, Y., and Noguchi, T. (2016) Role of a water network around the Mn_4CaO_5 cluster in photosynthetic water oxidation: A Fourier transform infrared spectroscopy and quantum mechanics/molecular mechanics calculation study. *Biochemistry 55*, 597−607.
(62) Nakamura, S., and Noguchi, T. (2017) Infrared determination of the protonation state of a key histidine residue in the photosynthetic water oxidizing center. *J. Am. Chem. Soc. 139*, 9364−9375.
(63) Miller, A.-F., and Brudvig, G. W. (1991) A guide to electron paramagnetic resonance spectroscopy of photosystem II membranes. *Biochim. Biophys. Acta, Bioenerg. 1056*, 1−18.
(64) Hwang, H. J., Dilbeck, P., Debus, R. J., and Burnap, R. L. (2007) Mutation of arginine 357 of the CP43 protein of photosystem II severely impairs the catalytic S-state cycle of the H_2O oxidation complex. *Biochemistry 46*, 11987−11997.
(65) Nagao, R., Ueoka-Nakanishi, H., and Noguchi, T. (2017) D1-Asn-298 in photosystem II is involved in a hydrogen-bond network near the redox-active tyrosine Y_Z for proton exit during water oxidation. *J. Biol. Chem. 292*, 20046−20057.
(66) Askerka, M., Brudvig, G. W., and Batista, V. S. (2017) The O_2-evolving complex of photosystem II: recent insights from quantum mechanics/molecular mechanics (QM/MM), extended X-ray absorption fine structure (EXAFS), and femtosecond X-ray crystallography data. *Acc. Chem. Res. 50*, 41−48.
(67) Suga, M., Akita, F., Hirata, K., Ueno, G., Murakami, H., Nakajima, Y., Shimizu, T., Yamashita, K., Yamamoto, M., Ago, H., and Shen, J.-R. (2015) Native structure of photosystem II at 1.95 Å resolution viewed by femtosecond X-ray pulses. *Nature 517*, 99−103.
(68) Service, R. J., Yano, J., Dilbeck, P. L., Burnap, R. L., Hillier, W., and Debus, R. J. (2013) Participation of Glutamate-333 of the D1 polypeptide in the ligation of the Mn_4CaO_5 Cluster in photosystem II. *Biochemistry 52*, 8452−8464.
(69) Lohmiller, T., Cox, N., Su, J.-H., Messinger, J., and Lubitz, W. (2012) The basic properties of the electronic structure of the oxygen-evolving complex of photosystem II are not perturbed by Ca^{2+} removal. *J. Biol. Chem. 287*, 24721−24733.
(70) Kato, Y., Shibamoto, T., Yamamoto, S., Watanabe, T., Ishida, N., Sugiura, M., Rappaport, F., and Boussac, A. (2012) Influence of the PsbA1/PsbA3, Ca^{2+}/Sr^{2+} and Cl^-/Br^- exchanges on the redox potential of the primary quinone Q_A in photosystem II from *Thermosynechococcus elongatus* as revealed by spectroelectrochemistry. *Biochim. Biophys. Acta, Bioenerg. 1817*, 1998−2004.
(71) Cox, N., Rapatskiy, L., Su, J.-H., Pantazis, D. A., Sugiura, M., Kulik, L., Dorlet, P., Rutherford, A. W., Neese, F., Boussac, A., et al. (2011) Effect of Ca^{2+}/Sr^{2+} substitution on the electronic structure of the oxygen-evolving complex of photosystem II: a combined multifrequency EPR, ^{55}Mn-ENDOR, and DFT study of the S_2 state. *J. Am. Chem. Soc. 133*, 3635−3648.
(72) Beck, W. F., de Paula, J. C., and Brudvig, G. W. (1986) Ammonia binds to the manganese site of the oxygen-evolving complex of photosystem II in the S_2 state. *J. Am. Chem. Soc. 108*, 4018−4022.
(73) Stich, T. A., Yeagle, G. J., Service, R. J., Debus, R. J., and Britt, R. D. (2011) Ligation of D1-His332 and D1-Asp170 to the manganese cluster of photosystem II from *Synechocystis* assessed by multifrequency pulse EPR spectroscopy. *Biochemistry 50*, 7390−7404.
(74) Kern, J., Chatterjee, R., Young, I. D., Fuller, F. D., Lassalle, L., Ibrahim, M., Gul, S., Fransson, T., Brewster, A. S., Alonso-Mori, R., Hussein, R., Zhang, M., Douthit, L., de Lichtenberg, C., Cheah, M. H., Shevela, D., Wersig, J., Seuffert, I., Sokaras, D., Pastor, E., Weninger, C., Kroll, T., Sierra, R. G., Aller, P., Butryn, A., Orville, A. M., Liang, M., Batyuk, A., Koglin, J. E., Carbajo, S., Boutet, S., Moriarty, N. W., Holton, J. M., Dobbek, H., Adams, P. D., Bergmann, U., Sauter, N. K., Zouni, A., Messinger, J., Yano, J., and Yachandra, V. K. (2018) Structures of the intermediates of Kok's photosynthetic water oxidation clock. *Nature 563*, 421−425.

NOTE ADDED AFTER ASAP PUBLICATION

This article was published ASAP on February 15, 2019. The Table of Contents/Abstract graphic has been updated and was reposted on February 19, 2019.

DOI: 10.1021/acs.biochem.8b01184
Biochemistry 2019, 58, 1379−1387